Short-amplitude high-frequency wing strokes determine the aerodynamics of honeybee flight

Douglas L. Altshuler*, William B. Dickson*, Jason T. Vance†, Stephen P. Roberts†, and Michael H. Dickinson*‡

*Bioengineering, Mail Code 138-78, California Institute of Technology, 1200 East California Boulevard, Pasadena, CA 91125; and †Department of Biological Sciences, University of Nevada, 4505 South Maryland Parkway, Las Vegas, NV 89154-4004

Most insects are thought to fly by creating a leading-edge vortex that remains attached to the wing as it translates through a stroke. In the species examined so far, stroke amplitude is large, and most of the aerodynamic force is produced halfway through a stroke when translation velocities are highest. Here we demonstrate that honeybees use an alternative strategy, hovering with relatively low stroke amplitude (≈90°) and high wingbeat frequency (≈230 Hz). When measured on a dynamically scaled robot, the kinematics of honeybee wings generate prominent force peaks during the beginning, middle, and end of each stroke, indicating the importance of additional unsteady mechanisms at stroke reversal. When challenged to fly in low-density heliox, bees responded by maintaining nearly constant wingbeat frequency while increasing stroke amplitude by nearly 50%. We examined the aerodynamic consequences of this change in wing motion by using artificial kinematic patterns in which amplitude was systematically increased in 5° increments. To separate the aerodynamic effects of stroke velocity from those due to amplitude, we performed this analysis under both constant frequency and constant velocity conditions. The results indicate that unsteady forces during stroke reversal make a large contribution to net upward force during hovering but play a diminished role as the animal increases stroke amplitude and flight power. We suggest that the peculiar kinematics of bees may reflect either a specialization for increasing load capacity or a physiological limitation of their flight muscles.

bee flight | flight in heliox | stroke amplitude | unsteady mechanisms | wingbeat kinematics

In 1934, August Magnan and André Sainte-Lague (1) concluded from a simple mathematical analysis that the flight of bees was "impossible." Since this time, bees have symbolized both the inadequacy of aerodynamic theory as applied to animals and the hubris with which theoreticians analyze the natural world. Although the assumptions used by Magnan and Sainte-Lague have since proven erroneous (2), conventional fixed-wing aerodynamic theory is indeed insufficient to explain the flapping flight of bees and other small insects. In particular, the performance of insect wings, when tested under steady conditions in wind tunnels, is too low to account for the forces required to sustain flight (3). However, a number of more recent studies have demonstrated that wings perform much better when started from rest or rotated continuously around their base (4–6) due to the formation of a leading-edge vortex (LEV). Instead of shedding to initiate stall, the LEV remains attached throughout each stroke, presumably because of the transport of vorticity by span-wise flow (7–9). Whereas the delayed stall forces are greatest at midstroke, flapping wings generate additional forces during stroke reversals. These forces, which result from the rapid rotation of the wing, added mass effects, and the influence of the wake shed from previous strokes, are very sensitive to the precise pattern of wing motion (5, 10). In many insects, including fruit flies (*Drosophila*), wing stroke amplitude is large (≈145–165°), and translational forces dominate those generated during stroke reversal (11, 12). However, numerous bee species [*Bombus* (13), *Xylocopa* (14), and Euglossine tribe (15)] hover with shallow strokes (<130°) separated by rapid reversals. The aerodynamic, physiological, and ecological significance of this small-amplitude stroke pattern is not known.

Aerodynamic forces are proportional to the square of wing tip velocity, itself a product of stroke amplitude, wingbeat frequency, and wing length. Thus, a bee hovering with reduced stroke amplitude could compensate by increasing its stroke frequency to achieve roughly equivalent average forces to an animal flapping with a higher stroke amplitude and lower stroke frequency. Several investigators have documented that many bee species do indeed use high stroke frequency relative to their body size (16). For example, honeybees *Apis mellifera*, with an average wing length of 9.7 mm, beat their wings 240 time per second (17). By comparison, a much smaller fruit fly, *Drosophila melanogaster*, flaps its 2.5-mm wings 200 times per second.

The first goal of the present study was to capture the detailed free-flight hovering kinematics of *A. mellifera* by using a multi-camera high-speed digital video system. We then measured the time course of aerodynamic force production by using a dynamically scaled robotic model to determine the relative importance of different force generating mechanisms. Next, we measured how bees manipulate their low-amplitude high-frequency stroke pattern to increase flight output when flying in low-density heliox. Finally, we determined the aerodynamic consequences of these changes in wing motion by measuring the forces generated by artificial kinematic patterns based on those used by aerodynamically challenged bees.

Methods

Filming of Free Hovering in Air and in Heliox. Honeybees (*A. mellifera*) of the forager caste were captured on exiting a hive located at the University of Nevada, Las Vegas. We chose to use outgoing foragers, in part to minimize the variance in nectar or pollen loads carried by equally sized bees. Up to three bees were captured within several minutes and then immediately transferred to a cubic chamber made of transparent acrylic (each side, 25 cm). The air temperature was room temperature (24–25°C). A 250-ml glass beaker was placed centrally within the cube in an inverted position to provide a focal platform. Drops of high-molarity sucrose solution and pinches of pollen grains were placed on top of the platform to provide a flight target as well as sustenance. However, we did not observe any engorgement or loading that would have resulted in substantial changes in bee weight. We allowed the bees to move freely within the chamber until a good hovering sequence was captured by all three cameras or until the bees displayed by sufficient lethargy or disinterest that further hovering flights were unlikely.

We used three high-speed digital cameras (Photron APX, San Diego, CA) to capture honeybee flights at 6,000 frames per

PHYSIOLOGY

second at a spatial resolution of 512 × 512 pixels. The cameras were positioned orthogonally and synchronized by a master central processing unit. In each trial, we collected 3 seconds of data.

If we captured an acceptable hovering sequence in normal air within 5–10 min of initial release into the chamber, we then replaced the chamber contents with a 21%:79% oxygen/helium mixture (normoxic heliox). Complete gas replacement was accomplished within 10 min. Because normoxic heliox has a much lower air density ($\rho = 0.41$ kg/m^3) than ambient air ($\rho = 1.21$ kg/m^3), this treatment forces the bees to generate higher aerodynamic power for hovering (18). We then attempted to film the bees in heliox until all three animals in the chamber exhibited lethargy or disinterest.

Wing and Body Digitization. Still frames from the digital cameras were analyzed in sequence by using custom software (11). Because the cameras were aligned orthogonally, spatial calibration was performed by using anatomical features on the honeybee itself that were visible in all three frames. Six points were located in each frame by using at least two camera views: head, tail, and wing tips and wing hinges for both left and right sides. A plane determined by regression through the wing-tip path was defined as the stroke plane. Position of the wing tips relative to the wing hinges was used to calculate the stroke position angles within the stroke plane (ϕ) as well as the deviation angle from the stroke plane (θ). The angular orientation of the wing (angle of attack, α) was digitized by rotating and aligning a wire-frame image of a honeybee wing over all three views until optimal overlap was achieved by visual inspection. Graphical depictions of the honeybee planform and the wing angle system are available in supporting information, which is published on the PNAS web site. The time course of the wing angles was smoothed by using a cubic spline (19).

Construction of Artificial Kinematics. The average wingbeat patterns were calculated for the bees in normal air and in heliox. The left and right wing kinematics for each bee were partitioned into single cycles consisting of one upstroke and one downstroke. Average wing angles were calculated after scaling each cycle to the mean cycle period to provide a common time base.

The ability of the dynamically scaled robotic model to produce essentially arbitrary kinematic trajectories provided us with the opportunity to systematically examine how aerodynamic forces vary with stroke amplitude. We generated artificial trajectories based on the mean wingbeat kinematics in normal air by systematically varying the stroke amplitude from 80° to 180° in 5° increments. Two methods for scaling wingtip velocity with stroke amplitude were considered. In the first case, the period was scaled to maintain a constant rate of change in instantaneous stroke position for all amplitudes, hereafter referred to as constant velocity trials. Thus, increases in stroke amplitude were offset by decreases in wingbeat frequency. In the second case, the stroke period was held constant for all amplitudes so that wingtip velocity increased with stroke amplitude, hereafter referred to as constant frequency trials. As will be shown, this latter protocol more closely matches the behavioral response of bees to increased aerodynamic load.

Aerodynamic Force Measurements. The aerodynamic forces produced by hovering honeybees as well as artificially generated kinematics were measured by using a dynamically scaled robot. An appropriate dynamic scaling can be achieved between the forces produced by the robot and the hovering honeybee by matching the Reynolds numbers (Re) for the two systems (11, 12), where Re is given by the product of mean wing chord and tip velocity divided by the kinematic viscosity. A full description of the robotic apparatus has been presented elsewhere (5, 10),

and only a brief description will be provided here. A model planform of a honeybee wing was made from 2-mm-thick acrylic and mounted to a two-axis force sensor at the base of the wing that measured forces normal and parallel to the wing surface. Forces were sampled at 500 Hz by using a multifunction analog/digital card. The entire length of the wing and the sensor was 25 cm from the axis of rotation. The wing and sensor were attached to a robotic arm that provided three degrees of motion actuated by three servo motors and controlled by a personal computer. The wing and the robotic arm were submerged in mineral oil with a fluid density of 830 kg/m^3 and a kinematic viscosity of 11 centistokes.

The raw force data were filtered offline by using a fourth-order zero-phase low-pass filter (Butterworth) with a cutoff frequency of 5 Hz. Instantaneous measures of lift and drag forces were derived from parallel and normal wing forces by using trigonometric relations. In addition to measuring forces for the natural and artificial wingbeat kinematics, we also measured the steady-state lift and drag forces for a bee planform undergoing steady rotation at a fixed angle of attack at a Re of 970. Measurements were made for angles of attack from −9° to 99° in 4.5° increments. For each angle of attack, the wing revolved through 240° at a constant angular velocity, and the mean force from the portion of the stroke from 96° to 168° was used for calculations of steady-state force coefficients (as in ref. 5).

For comparing the effects of stroke amplitude in the artificial wingbeat kinematics, we used steady-state force coefficients to estimate the aerodynamic forces due to the instantaneous angle of attack and translational velocity of the wing (20). This quasi-steady estimate does not include forces due to wing rotation, added mass, or wake capture. Therefore, differences between the estimated and measured forces indicate when the forces deviate from the steady-state predictions of the translational force coefficients. This was quantified by calculating the root mean square difference between measured and estimated forces, and dividing the sum of this difference by the total measured force at each amplitude, to provide a single metric that could be compared across stroke amplitudes.

Results

Free-Flight Wingbeat Kinematics. We analyzed the hovering wingbeat kinematics of four bees from separate trials. Because up to three bees were present in the chamber during each trial, body morphometrics were averaged. Four additional bees were analyzed after replacing chamber contents with heliox. Because we could not identify individual bees, it is possible that some of the same bees may have been analyzed for both hovering and heliox. A representative hovering sequence in normal air is presented in Fig. 1. The time course for stroke position reveals that wings extend much further behind the wing hinge $\bar{X} = 76.0° \pm 6.7°$ SD) than in front of it $\bar{X} = 19.3° \pm 4.8°$ SD). The time courses of angle of attack and stroke deviation are remarkably similar to the wingbeat kinematics of hovering fruit flies (11). For example, in both honeybees and fruit flies, stroke deviation oscillates at twice the wingbeat frequency with upward peaks occurring at stroke reversal to create a ''U-shaped'' trajectory. In normal air, the bees hovered with an average wingbeat frequency of 230 Hz and shallow stroke amplitude of only 91° (Table 1). In heliox, bees maintained wingbeat frequency but increased stroke amplitude to an average value of 132°.
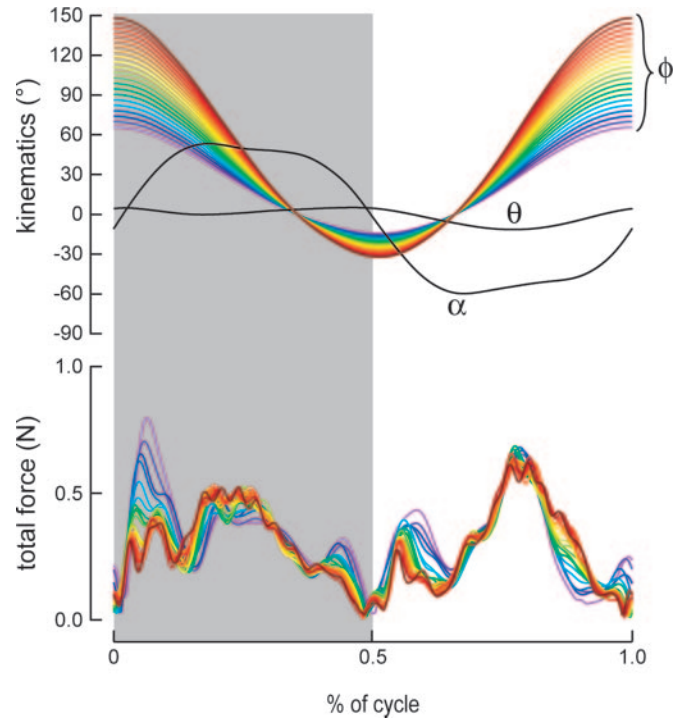
Aerodynamic Force Production. The forces generated by replaying the free-flight hovering kinematics through the robot are presented in the lower trace of Fig. 1. Lift and drag follow a similar time course that is very different from equivalent traces measured for hovering fruit flies (11, 12), which flap with a broader stroke amplitude but slower wingbeat frequency. Whereas the fly forces are dominated by translational components at mid-
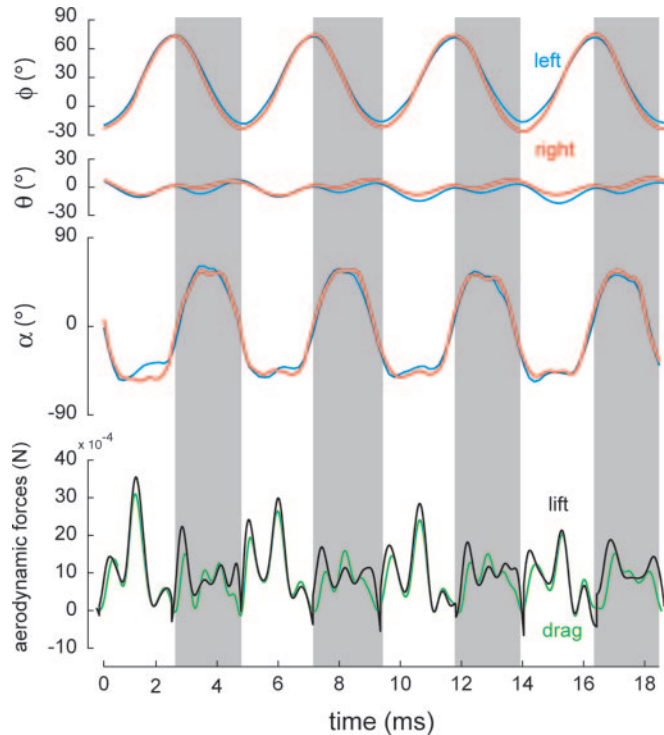
Fig. 1. The kinematics and aerodynamics of honeybee hovering. Representative data are presented for one individual during four wingbeats with the downstroke shaded in gray. The time course of both the left (blue trace) and right (red trace) wings is presented for three position angles: stroke position (ϕ), stroke deviation (θ), and geometric angle of attack (α). The lift (black trace) and drag (green trace) forces are presented for the left wing's kinematics, although the forces produced by the right wing kinematics were qualitatively similar. Forces have been scaled to honeybee dimensions (12).

Fig. 2. Changes in aerodynamics forces with increasing stroke amplitude, part I: constant mean wingtip velocity. The effects of stroke amplitude were tested by stepping through amplitudes from 80° to 180° in 5° increments that are color-coded in the time course for stroke position (ϕ). The average wingtip velocity was held constant by adjusting wingbeat frequency in inverse proportion to changes in stroke amplitude. The periods of stroke deviation (θ) and angle of attack (α) were adjusted to match that of ϕ. The total aerodynamic forces are plotted (*Lower*) with traces color-coded to equivalent ϕ-kinematics from *Upper*.

stroke, which are well described by a quasisteady approximation, the bee force trajectory includes major peaks at the beginning, middle, and end of each stroke. We investigated the transition between these two force-time histories (i.e., "fly-like" and "bee-like") by creating a set of artificial kinematics patterns with variable amplitude but constant velocity (Fig. 2). The magnitudes of total aerodynamic force are similar during the middle of each stroke regardless of the magnitude of stroke amplitude. However, the peak magnitude of the force transients at the beginning and end of each stroke falls off rapidly as the kinematics transition from a bee- to a fly-like pattern. Furthermore, increases in stroke amplitude above 135° (yellow trace) resulted in little changes in the time history of forces at stroke reversal.

In another set of experiments with artificial kinematics, we varied stroke amplitude while maintaining constant frequency.

This set mimics the transition in stroke pattern in hovering bees when they are moved from normal air to heliox (Fig. 3). In contrast to the constant velocity trials, the forces measured with constant frequency grew with increasing stroke amplitude, as expected from the rise in mean wingtip velocity. We could not make measurements for amplitudes above 135° because the force magnitudes exceeded the capacity of the force sensor on the robotic wings. Nevertheless, the trend in forces with rising stroke amplitude is clear.

To estimate the forces due to constant-velocity wing sweep, we calculated the lift-and-drag coefficients from measurements of revolving wings at constant velocity (Fig. 4). For these measurements, a Re was selected to match one of the bees hovering in normal air. The Re varied among the bees in normoxic air by at most 20%, and over this range, the nondimensional force

Table 1. The wingbeat frequency (n, Hertz), stroke amplitude (Φ, degrees), and Re of honeybees hovering in normal air (21%O_2, 79%N_2, $\rho = 1.21$ kg/m^3) and in heliox (21%O_2, 79%He, $\rho = 0.41$ kg/m^3)

	Normal air				Heliox		
Bee	n, Hz	Φ, °	Re	Bee	n, Hz	Φ, °	Re
1	221.5 ± 4.6	93.9 ± 5.1	1,124	5	252.2 ± 4.6	116.1 ± 4.5	1,582
2	227.7 ± 11.0	96.7 ± 6.8	1,189	6	232.0 ± 5.7	151.7 ± 2.5	1,901
3	245.0 ± 5.3	89.0 ± 9.3	1,177	7	224.4 ± 4.0	147.2 ± 2.8	1,784
4	227.6 ± 4.4	81.3 ± 4.8	1,000	8	231.8 ± 5.1	118.4 ± 3.4	1,483
x̄	229.8 ± 11.0	90.8 ± 8.6	1,123 ± 81.3	x̄	235.8 ± 11.7	131.6 ± 16.6	1,687 ± 190

Kinematics for four bees in each treatment were calculated for a total of eight bees. Individual averages (mean ± SD) for five strokes of each bee as well as treatment averages are presented.

PHYSIOLOGY
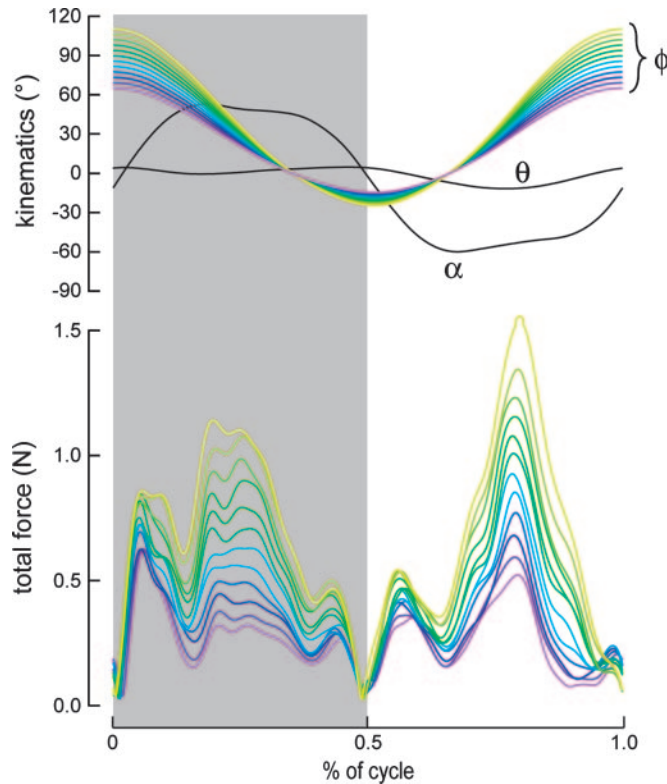
Fig. 3. Changes in aerodynamics forces with increasing stroke amplitude, part II: constant wingbeat frequency. The wingbeat frequency was held constant at the mean value for hovering across stroke amplitudes from 80° to 135° in 5° increments. Stroke amplitudes above 135° were not tested because the magnitudes of peak forces exceeded the capacity of the force sensor. However, the color-coding scheme for wingbeat kinematics (*Upper*) is the same as for Fig. 2. The total aerodynamic forces are plotted (*Lower*) with traces color-coded to equivalent ϕ kinematics from *Upper*.

coefficients did not measurably differ. From these measurements, we could calculate a quasi-steady estimate for the force created by any arbitrary pattern of wing motion. The quasisteady
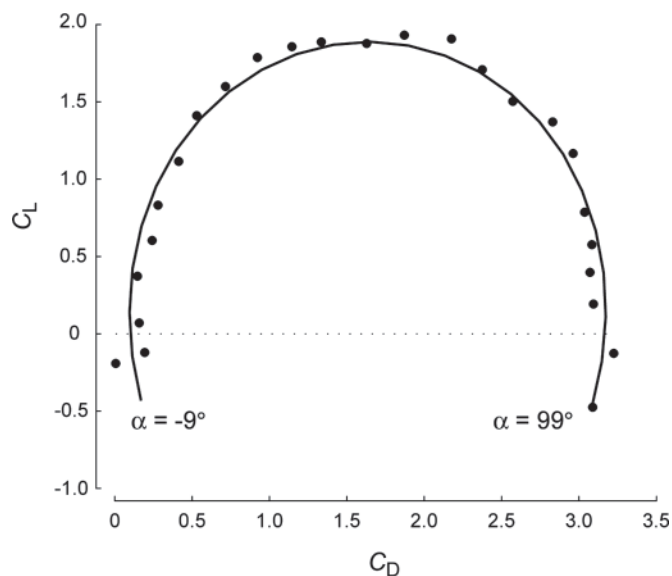
Fig. 4. Lift coefficient (C_L) versus drag coefficient (C_D) as a function of angle of attack (α) for a honeybee wing planform at Re 970.

estimates poorly predict the measured forces at low stroke amplitudes, but the prediction improves as stroke amplitude increases for both the constant velocity and constant frequency cases (Fig. 5A). This indicates that unsteady effects operating at stroke reversal become increasingly important at low-stroke amplitude. Representative strokes are depicted for the 80° amplitude stroke (Fig. 5B), as well as the largest strokes recorded for the constant frequency ($\Phi = 135°$, Fig. 5C) and constant velocity ($\Phi = 180°$, Fig. 5D) experiments.

Discussion

Honeybees hover using a shallow stroke amplitude and high wingbeat frequency that produces multiple force peaks during each wingbeat (Fig. 1). The presence of high-magnitude force transients at the onset and termination of each stroke suggests that rotational, acceleration-reaction, and wing-wake interaction forces are more important for bees than for insects using high-amplitude low-frequency strokes, such as fruit flies (Fig. 2). This hypothesis was tested by experimentally extending the stroke amplitude on a robotic model while decreasing wingbeat frequency to maintain a constant wing-tip velocity. The results indicate that relative contribution of the unsteady forces at stroke reversal increases monotonically as stroke amplitude decreases for stroke amplitudes <135°. Thus, hovering honeybees make greater use of unsteady mechanisms at stroke reversal than all other insects examined so far.

Honeybees are able to increase power output, as indicated by placing them in a heliox mixture that is equivalent to the air density at an altitude of ≈9,200 m. This capability has also been described in orchid bees (18) and at least some individual carpenter bees (14) and may be a common feature among Apids. The honeybees in our study responded to heliox with a 48% increase in stroke amplitude but only a 2% increase in frequency, relative to normal air. We examined the aerodynamic consequences of this change in wing motion by playing a set of kinematic patterns on the dynamically scaled robot in which stroke frequency remained constant as stroke amplitude increased (Fig. 3). Whereas the unsteady force transients changed little as stroke amplitude increased, the midstroke forces grew extensively. These results indicate that bees make extensive use of unsteady stroke-reversal forces when hovering under benign conditions but raise stroke amplitude, while maintaining constant frequency, to increase the relative contribution of translational forces.

For all of the kinematic patterns we examined, the forces created by large-amplitude strokes were reasonably well approximated by a quasisteady model based upon empirically measured steady-state force coefficients. The transients at stroke reversal, which are more prominent at low stroke amplitude, may be due to a combination of aerodynamic effects. One important component is the added mass, also described as acceleration-reaction force (21). The effect of added mass is evident in the influence of stroke amplitude on the magnitude of reversal transients when tip velocity is held constant (Fig. 2). The increase in acceleration before and after stroke reversals at low stroke amplitude results in larger added mass forces. In contrast, when frequency is held constant, both velocity and acceleration rise with amplitude. However, because the translational force scales as the square of velocity, whereas the acceleration-reaction force scales linearly with acceleration, the relative contribution of the added mass is greater for shorter amplitude strokes. The forces during stroke transition are also influenced by wake capture, in which a wing encounters the shed vorticity from its previous stroke (4, 5, 22), and the Kramer effect (23), in which changes in angle of attack create circulation as the wing moves (5, 10). Although it is difficult to experimentally separate these unsteady effects, they presumably all contribute to the forces during stroke reversal.
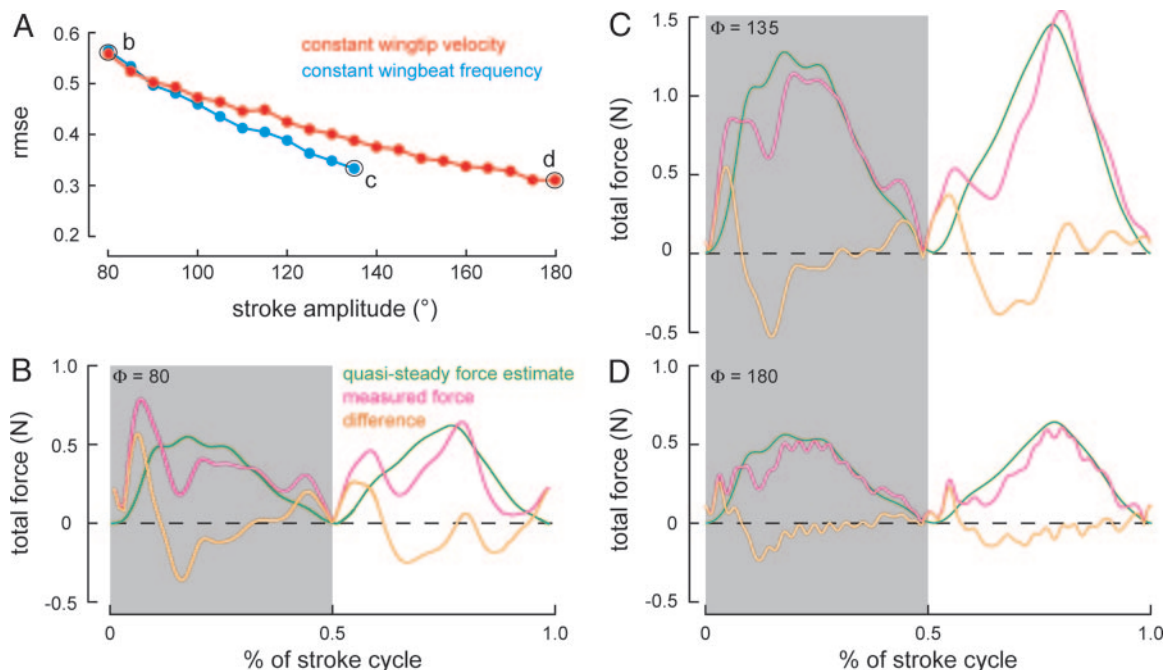
Fig. 5. Unsteady aerodynamic effects with decreasing stroke amplitude. The forces produced by wing translation were calculated by using the quasi-steady estimate of Sane and Dickinson (20), and the rms error between the total measured forces and estimated translational forces is plotted across stroke amplitudes in *A*. The time courses of measured forces, estimated translational forces, and instantaneous difference between these values are presented for three cases: stroke amplitude of 80° (*B*), stroke amplitude of 135° for the constant frequency case (*C*), and stroke amplitude of 180° for the constant velocity case (*D*).

Among all features of the wingstroke, values for stroke amplitude and wingbeat frequency are known for the greatest number of taxa. Experiments on many groups of hovering animals indicate a general trend in which wingbeat frequency is highly correlated with body morphology, particularly wing length, whereas stroke amplitude is largely size-independent (15, 16, 24, 25). However, these relationships contain consistent patterns of outliers from the overall trend, which led Greenewalt (16) to identify four major groupings of insects distinguished according to their relationship to the mean regression. Greenewalt's group 1, which exhibit unusually high wingbeat frequencies relative to their body sizes, includes the hymenopteran genera *Apis* and *Bombus*. Members of group 4, which include *Drosophila*, exhibit unusually low wingbeat frequencies relative to body size.

In a prior study, a dynamically scaled robot was used to study instantaneous flight forces within a broad kinematic parameter space that bracketed the full range of stroke amplitudes used by honeybees and fruit flies (10). This analysis unequivocally demonstrates that kinematics with low stroke amplitudes are less aerodynamically efficient as measured by lower mean lift-to-drag and lift-to-power ratios. Given this result, it is quite curious why honeybees, which, given their foraging habits, should be under severe selection for transport efficiency, should hover using an intrinsically inefficient stroke. Possible explanations for this paradox emerge by considering the physiological constraints (proximate mechanisms) as well as behavioral ecology (ultimate causes) of these central-place foragers.

The theoretical maximum value for stroke amplitude occurs when the wings encounter each other during pronation and supination, but the thoracic geometry itself may impose a lower limit. For example, many bees apparently reach maximum stroke amplitude at angles of ≈140° (24). Stroke frequency, in turn, is limited by several factors, including wing mass, thoracic mechanics (26), and the physiological properties of the muscles (27). Contractile frequencies are influenced by temperature, although

optimal temperatures are in turn a function of several properties including muscle type and calcium sensitivity. All these features appear to be highly taxon-specific. For example, the bees *Bombus* and *Apis* (Greenewalt's group 1) perform maximally at flight muscle temperatures near 40°C (28, 29), although these can fly with muscle temperatures as low as 25°C. Fruit flies (group 4) are capable of flight at even lower flight muscle temperatures (≈15°C) and approach optimal muscle performance at muscle temperatures of 25°C (30). Others properties of the muscular-skeletal system can influence mechanical efficiency. However, any discussion of mechanical power expenditure must, by definition, include inertial costs of accelerating and decelerating the wing (31). These costs can be offset by elastic energy storage (32) or conversion to aerodynamic power (12, 33) but are essentially unknown for all but a few taxa.

Although honeybees increase aerodynamic force production by modulating stroke amplitude, this is not the only avenue that is theoretically available. Increases in wingbeat frequencies have been demonstrated in other insects with asynchronous flight muscles such as *D. melanogaster*, which do so in tethered preparations (34). All asynchronous flight muscle should display a unimodal frequency tuning (35). Power output is equal to the product of frequency and the area enclosed by a shortening/lengthening cycle within a stress-strain "work loop." Although power initially rises with frequency, the work per cycle declines with rising frequency due to the inability of crossbridges to detach quickly enough at the onset of lengthening. One prediction that emerges from this study is that bee muscle exhibit a narrower frequency tuning than does fly muscle. For this reason, the neuromechanical control system functions to maintain stroke frequency at a nearly constant value. Thus, there might exist two distinct physiological features of bee muscles: a peak mechanical output that is shifted to higher temperature and narrowly tuned to high frequency. If so, then variation in wingbeat frequencies from other studies (≈200–250) should be an attributable difference in temperature and/or wing length (13, 16). This hy-

pothesis could be testable with further biophysical and molecular studies.

An ecological explanation for the lower-efficiency stroke of honeybees is that, because these insects consume floral nectar, they may have excess power available for ecological useful but aerodynamically expensive behaviors, as do hovering humming-birds that are able to forage for high-energy nectar rewards by using more energetically demanding flight. Honeybees and other hymenopterans need to carry much heavier loads that may actually exceed body mass in numerous contexts, including undertaking, prey transport, and foraging for nectar or pollen. The ability to lift loads in excess of body mass has been demonstrated for many species of insects, although the broadest comparisons concern maximal loads that are only transiently lifted (15, 36). However, some data are available concerning the kinematics and metabolic performance associated with foraging flight. Feuerbacher *et al.* (37) measured free-flight kinematics in honeybees during pollen loading and found that they used higher stroke amplitude ($\Phi = 118°$) with essentially the same wingbeat frequencies ($n = 234$ Hz) as recorded here. However, these values did not change depending upon the weight of the pollen load. Load size also had no influence on metabolic rate in this same study, although increases in oxygen consumption with larger nectar loads have been recorded elsewhere (38). The results from honeybees are consistent with a study of bumblebees that showed increases in flight speed (which should raise parasite drag) require little increase in metabolic rate (39). Further studies have shown that motivational drive may drive increases in oxygen consumption more than excess load (40, 41). Thus, foraging flights do require enhanced performance relative to baseline hovering, but the specific influence of load size on both biomechanics and physiology is not yet understood.

In conclusion, our analysis of honeybee aerodynamics reveals how the rapid low-amplitude wing motion of bees is sufficient to maintain the weight of the animal. Furthermore, honeybees exhibit considerable ability to generate excess aerodynamic power, which they accomplish by raising stroke amplitude while maintaining constant frequency. This ability may be related to requirements of social insects to carry loads related to foraging, undertaking, and brood transport.

1. Magnan, A. (1934) *La Locomotion Chez les Animaux* (Hermann, Paris), Vol. 1.
2. McMasters, J. H. (1989) *Am. Sci.* **March–April,** 164–169.
3. Ellington, C. P. (1984) *Philos. Trans. R. Soc. London B* **305,** 1–15.
4. Dickinson, M. H. & Götz, K. G. (1993) *J. Exp. Biol.* **174,** 45–64.
5. Dickinson, M. H., Lehmann, F.-O. & Sane, S. P. (1999) *Science* **284,** 1954–1960.
6. Usherwood, J. R. & Ellington, C. P. (2002) *J. Exp. Biol.* **205,** 1547–1564.
7. Ellington, C. P., van den Berg, C., Willmott, A. P. & Thomas, A. L. R. (1996) *Nature* **384,** 626–630.
8. Birch, J. M. & Dickinson, M. H. (2001) *Nature* **412,** 729–733.
9. Birch, J. M., Dickson, W. B. & Dickinson, M. H. (2004) *J. Exp. Biol.* **207,** 1063–1072.
10. Sane, S. P. & Dickinson, M. H. (2001) *J. Exp. Biol.* **204,** 2607–2626.
11. Fry, S. N., Sayaman, R. & Dickinson, M. H. (2003) *Science* **300,** 495–498.
12. Fry, S. N., Sayaman, R. & Dickinson, M. H. (2005) *J. Exp. Biol.* **208,** 2303–2318.
13. Ellington, C. P. (1984) *Philos. Trans. R. Soc. London B* **305,** 41–78.
14. Roberts, S. P., Harrison, J. F. & Dudley, R. (2004) *J. Exp. Biol.* **207,** 993–1004.
15. Dillon, M. E. & Dudley, R. (2004) *J. Exp. Biol.* **207,** 417–425.
16. Greenewalt, C. H. (1962) *Smithsonian Misc. Coll.* **144,** 1–46.
17. Sotavalta, O. (1952) *Ann. Zool. Sci. Zool. Bot. Fenn. Van.* **15,** 1–66.
18. Dudley, R. (1995) *J. Exp. Biol.* **198,** 1065–1070.
19. Reinsch, C. H. (1967) *Num. Math.* **10,** 177–183.
20. Sane, S. P. & Dickinson, M. H. (2002) *J. Exp. Biol.* **205,** 1087–1096.
21. Sarpkaya, T. & Isaacson, M. (1981) *Mechanics of Wave Forces on Offshore Structures* (Van Nostrand Reinhold, New York).
22. Birch, J. M. & Dickinson, M. H. (2003) *J. Exp. Biol.* **206,** 2257–2272.
23. Ellington, C. P. (1984) *Philos. Trans. R. Soc. London B* **305,** 79–113.
24. Dudley, R. (2000) *The Biomechanics of Insect Flight: Form, Function, Evolution* (Princeton Univ. Press, Princeton, NJ).
25. Altshuler, D. L. & Dudley, R. (2003) *J. Exp. Biol.* **206,** 3139–3147.
26. Pringle, J. W. S. (1957) *Insect Flight* (Cambridge Univ. Press, Cambridge, MA).
27. Molloy, J. E., Kyrtatas, V., Sparrow, J. C. & White, D. C. S. (1987) *Nature* **328,** 449–451.
28. Gilmour, K. M. & Ellington, C. P. (1993) *J. Exp. Biol.* **183,** 77–100.
29. Coelho, J. R. (1991) *Physiol. Zool.* **64,** 823–825.
30. Lehmann, F. O. (1999) *J. Comp. Physiol. B* **169,** 165–171.
31. Casey, T. M. (1981) *J. Exp. Biol.* **91,** 117–129.
32. Jensen, M. & Weis-Fogh, T. (1962) *Philos. Trans. R. Soc. London B* **245,** 137–169.
33. Dickinson, M. H. & Lighton, J. R. B. (1995) *Science* **268,** 87–90.
34. Lehmann, F. O. & Dickinson, M. H. (1997) *J. Exp. Biol.* **200,** 1133–1143.
35. Josephson, R. K., Malamud, J. G. & Stokes, D. R. (2000) *J. Exp. Biol.* **203,** 2713–2722.
36. Marden, J. H. (1987) *J. Exp. Biol.* **130,** 235–258.
37. Feuerbacher, E., Fewell, J. H., Roberts, S. P., Smith, E. F. & Harrison, J. F. (2003) *J. Exp. Biol.* **206,** 1855–1865.
38. Wolf, T. J., Schmidhempel, P., Ellington, C. P. & Stevenson, R. D. (1989) *Funct. Ecol.* **3,** 417–424.
39. Ellington, C. P., Machin, K. E. & Casey, T. M. (1990) *Nature* **347,** 472–473.
40. Moffatt, L. (2000) *J. Comp. Physiol. A* **186,** 299–306.
41. Moffatt, L. & Nunez, J. A. (1997) *J. Comp. Physiol. B* **167,** 36–42.